Visualization of Horizontal Settling Slurry Flow Using Electrical Resistance Tomography

Kun Li, Mi Wang, and Yan Han

Abstract Settling slurry flow is very common and important in many industries, especially in transportation, which need to be monitored in practical operation. An investigation on visualization of horizontal settling slurry flow in pipeline using electrical resistance tomography was made in this paper. The internal images of fluid structure were displayed to operators with measurement of the solids concentration distribution and solids velocity distribution in pipe cross section. Experimental investigation with 5% solids loading concentration at various transport velocities was conducted. Meanwhile, the results of photography and other flow measurement methods were compared with the results obtained from electrical resistance tomography.

Keywords Flow visualization · Horizontal settling slurry flow · Electrical resistance tomography · Local solid concentration · Local solid velocity

1 Introduction

The transportation of settling slurry flow is required in a diverse range of industries, such as mining, nuclear, energy, pharmaceutical, chemical, and food industries [1–4]; especially in some specific applications, hydraulic transport through pipelines is the only method to transport solid particles. As the slurry is an essential mixture of solid and liquid, its characteristics rely on many factors, such as size and orientation of pipes, size and concentration of solids, velocity and viscosity of the liquid carrier. Slurry transportation is a highly complex process [2], which should be under measuring and monitoring in the transport process, and appropriate

K. Li (✉) · Y. Han
Shanxi Key Laboratory of Signal Capturing and Processing, North University of China, Taiyuan, China

M. Wang
School of Chemical and Process Engineering, University of Leeds, Leeds, UK

E. T. Quinto et al. (eds.), *The Proceedings of the International Conference on Sensing and Imaging, 2018*, Lecture Notes in Electrical Engineering 606,
https://doi.org/10.1007/978-3-030-30825-4_6

slurry flow parameters can efficiently avoid pipe blockage, equipment failures, and environmental damage. With well understanding the internal structure of the slurry flow, the optimal design, accurate analysis, and safe operation of slurry transportation systems can be more easily achieved.

Due to the complex nature of slurry flow and the effect of gravity, it is very difficult for measuring and visualizing settling slurry flow. In the past, venturimeter [5] based on differential pressure technique was widely used for measuring fluid flow rate. Conductivity probes [6] were installed inside pipes to measure the solids volumetric concentration, which disturbs the internal structure of slurry flow (i.e., intrusive method), and the abrasive nature of slurry makes the probe sensor to hardly survive. With significant efforts of worldwide researchers, several non-intrusive methods [7–10] appeared, such as, optical (laser), nuclear (X-ray or gamma ray), ultrasound, and conductance transducers. Among the above methods, electrical resistance tomography (ERT) offered a good solution for measuring and visualizing settling slurry flow, since the optical method cannot measure muddy fluid, and nuclear method is expensive and radioactive.

Phase volume fraction and phase velocity are two important parameters to describe the internal structure of slurry flow, and flow characteristics also can be extracted from them, for example, flow regimes [3]. With ERT online measurement, the real-time solids concentration and velocity distribution are offered, which allows process owners to "see" inside the pipe and determine flow conditions. The information can be used for understanding and managing slurry flow, and they also provide an experimental basis for CFD and other models in complex flows. Therefore, this paper focuses on the visualization of horizontal settling slurry flow, where local solids volumetric concentration and local solids axial velocity are measured with using an ERT system.

2 Horizontal Settling Slurry Flow Regimes

A flow regime describes the solids spatial distribution of settling slurry, which is crucial for design, optimisation, and the control of slurry flow processes. In horizontal settling slurry flow, with the influence of gravity and various flow velocities, the separation of phases occurs and four main flow regimes (from high velocity to low velocity) are developed, namely pseudo-homogeneous, heterogeneous, moving bed, and stationary bed [2], as shown in Fig. 1.

Homogeneous flow regime usually occurs at high velocities, where solids are fine particles and fully suspended in the liquid carrier, as shown in Fig. 1a. As the solid particles are almost equally distributed and flow with same velocity from top to bottom of pipe, it can be approximately regarded as single phase flow, which allows the equivalent fluid model used for representing the type of flow. This flow regime is the mostly used one in industrial applications. As the flow velocity decreases, heterogeneous flow regime occurs, where the solids concentration gradient and axis solid velocity gradient appears at the cross section of pipe. As shown in Fig. 1b, the

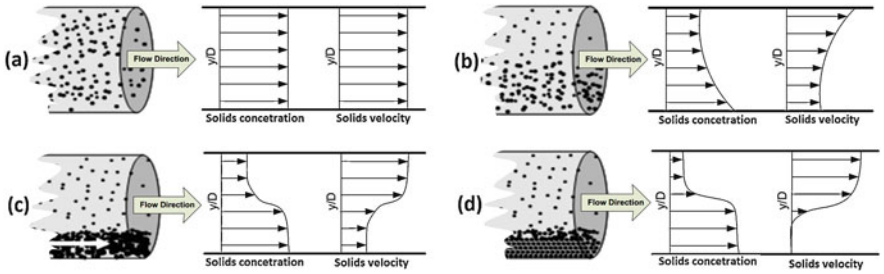

Fig. 1 Schematic presentations of horizontal slurry flow regimes with solids concentration and axis velocity profile. (**a**) Pseudo-homogeneous flow regime. (**b**) Heterogeneous flow regime. (**c**) Moving bed flow regime. (**d**) Stationary bed flow regime

flow regime is referred to as an intermediate flow regime, or might be in the process of forming a flowing bed, where some finer particles are suspended at top part of pipe and coarser particles are suspended at bottom part of pipe. The flow regime is usually applied in mining and dredging applications but a critical velocity is needed to maintain the flow regime, i.e., minimum velocity of liquid carrier. Moving bed flow regime starts to be formed when the flow velocity is below the critical velocity, where larger particles accumulate at the bottom of pipe and form a flowing bed, and the upper part of fluid is still heterogeneous mixture with less solids concentration, as shown in Fig. 1c. The solids concentration at bottom is maximum and decreases from bottom to top at cross section of pipe, while the solids velocity at upper part is higher than that at bottom part. As the flow velocity reduces further, the liquid carrier cannot move the solids on bed, which will be stationary and contact with the bottom of pipe, as shown in Fig. 1d. With the accumulation of solid particles, the stationary bed turns thicker, which might lead to blockage. Therefore, it is impossible for maintaining stationary bed flow regime for very long time, and it should be avoided in practice.

3 ERT System and Principle

The principle of ERT [11] is based on the concept of Ohm's law: by injecting a certain signal through electrodes pair into a conductive sensing region, and the injected signal will result in boundary voltages on the remaining electrodes. The boundary voltages contain the information of conductivity distribution which represents the phase distribution within the sensing region. Therefore, the boundary voltages data were collected and used to image the internal structure of multi-phase flow with using an image reconstruction algorithm [12].

A typical ERT system [11] is made of ERT sensor, data acquisition system, and image reconstruction system, as shown in Fig. 2. Each plane of ERT sensor is a set of equally spaced electrodes mounted around the pipe wall, which is in contact

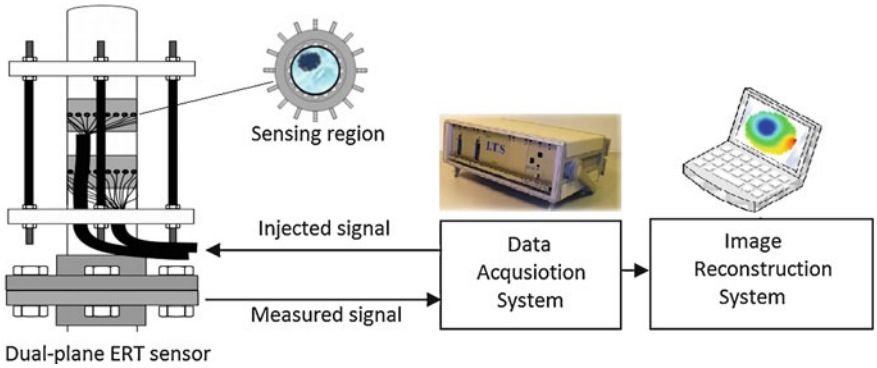

Fig. 2 Structure of ERT measurement system

with inside fluid, and does not cause any interference with the inside flow. The data acquisition system consists of signal sources, multiplexer arrays, voltmeters, signal demodulators, which is critical for ERT system since it determines sensing strategy, data accuracy, and highest data collection speed. Normally, an adjacent strategy [13] is used in most ERT systems, where a set of measured data contains 104 independent differential voltages for each 16-eletrode sensor. With using a preloaded image reconstruction algorithm, each set of measured data were transferred to each frame of internal conductivity distribution, which represents the phase distribution in the pipe cross section. The finite element mesh of pipe cross section is shown in Fig. 3.

Based on simplified Maxwell's relationship for slurry flow [14] (liquid carrier is water, and solids are silica sand in this paper), the obtained conductivity distribution can be used to derive the solids concentration distribution, as following Eq. (1).

$$\alpha = \frac{2\sigma_{\mathrm{w}} - 2\sigma_{\mathrm{m}}}{\sigma_{\mathrm{w}} + 2\sigma_{\mathrm{m}}} \tag{1}$$

where α is the solids concentration in each pixel, σ_{w} is the conductivity of continuous water phase, and σ_{m} is measured mixture conductivity of each pixel.

According to the internal conductivity distribution of dual plane, the pixel to pixel cross-correlation technique [15] is used to measure the time difference of solid particles flowing through two sensor planes, as shown in Fig. 4. With a predefined distance between them, the solids axial velocity can be calculated with using Eq. (2).

$$v = \frac{L}{T} \tag{2}$$

As the horizontal settling slurry flow without stirring can be assumed as vertically axial-symmetric, the solids concentration and velocity profile (Profile represents the distribution at vertical positions of pipe cross section) can be extracted using the average values of each row, i.e., Eqs. (3) and (4). And the local mean solids

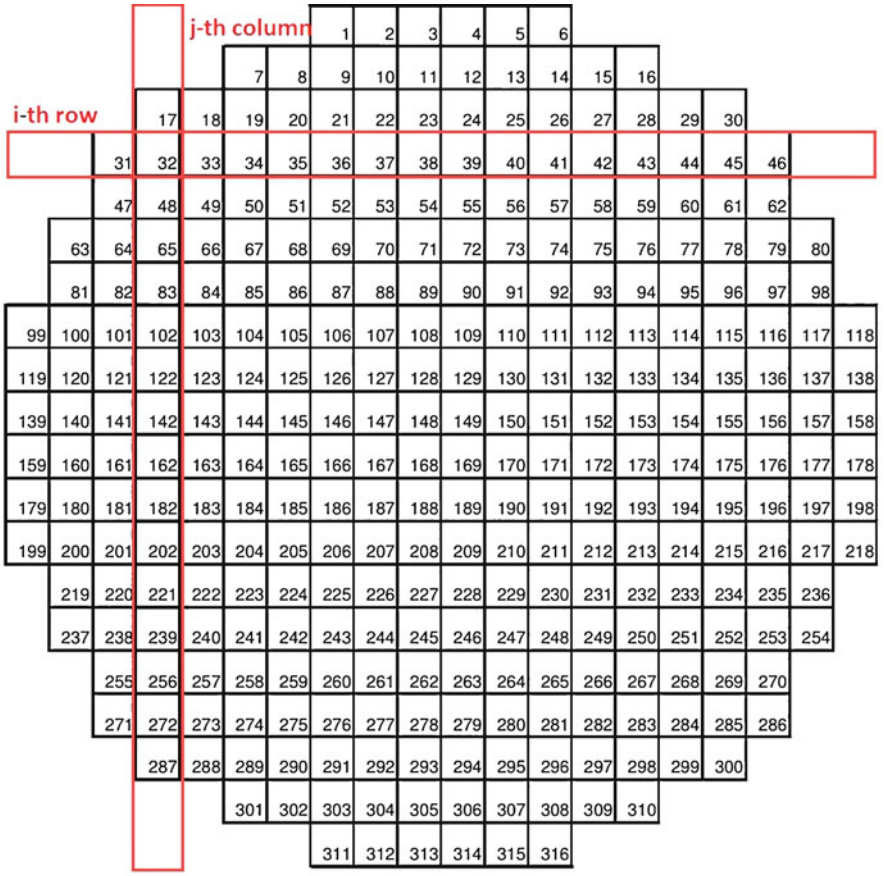

Fig. 3 Finite element mesh (*316 pixels*) of sensing region

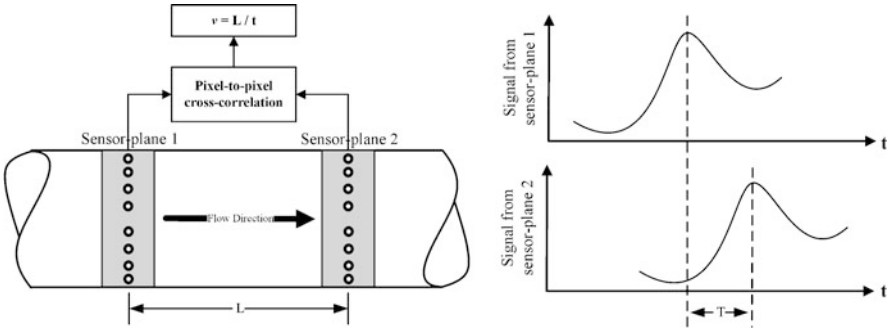

Fig. 4 Principle of pixel-to-pixel cross-correlation method

concentration and mean solids velocity can be calculated with the average value of 316 pixels, i.e., Eqs. (5) and (6).

$$\alpha_i = \frac{1}{n_i} \sum_{j=1}^{n_i} \alpha_{i,j} \tag{3}$$

$$v_i = \frac{1}{n_i} \sum_{j=1}^{n_i} v_{i,j} \tag{4}$$

$$\overline{\alpha} = \frac{1}{n} \sum \alpha_{i,j} \tag{5}$$

$$\overline{v} = \frac{1}{n} \sum v_{i,j} \tag{6}$$

where α_i and v_i are the average solids concentration and velocity of i-th row ($i = 1$, 2, ..., 20), respectively. $\overline{\alpha}$ and $\overline{v}$ are the local solids mean concentration and velocity, respectively. $\alpha_{i,j}$ and $v_{i,j}$ are the local solids concentration and velocity in the pixel of i-th row and j-th column, respectively.

4 Experiment Setup

Experimental investigation of settling slurry flow was conducted on a slurry flow loop facility in University of Leeds, as shown in Fig. 5. It consists of a high-performance dual-plane ERT system (FICA, built by OLIL) [16] for measuring local solids concentration and velocity, an EMF (OPTIFLUX 4300, from KROHNE) for obtaining fluid velocity, and a CMF (OPTIMASS 700 T50, from KROHNE) for obtaining slurry mass flow rate. The slurry flow run in experiment with 5% loading solids volumetric concentration at different transport velocity (from 1.5 to 4.0 m/s), where solid phase is silica sand (particle size is between 75 and 700 in diameter) and liquid carrier is tap water. Meanwhile, a section of transparent pipe was installed on slurry flow loop for taking photography of slurry flow at each transport velocity.

In order to evaluate the measurement and visualization of slurry flow using ERT, the photography results, EMF and CMF results were compared with ERT results. The solids concentration from CMF and EMF measurement can be calculated with Eq. (7).

$$\alpha \cdot \rho_s + (1 - \alpha) \cdot \rho_w = \frac{Q}{v \cdot A} \tag{7}$$

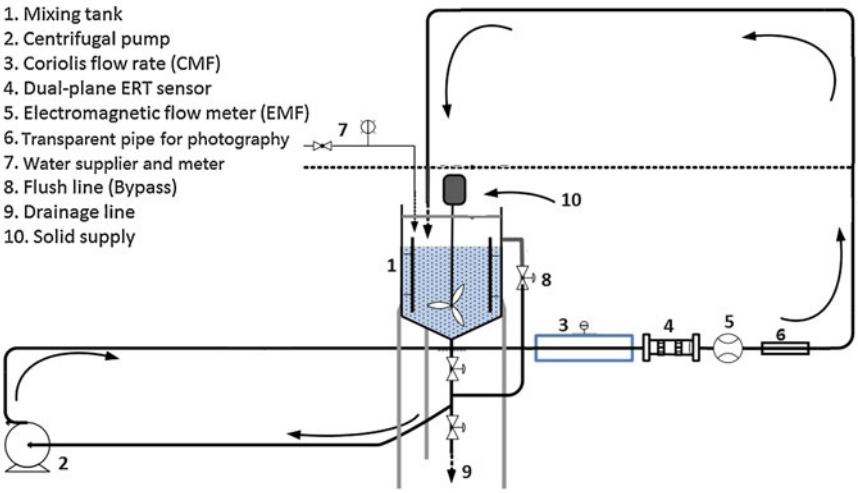

Fig. 5 Experimental facility (*slurry flow loop*) in Leeds University

where ρ_s and ρ_w are the density of sand and water, respectively. α is the solids concentration. Q and v are slurry mass flow rate and velocity, respectively. A is the area of pipe cross section.

5 Results and Discussions

Figure 6 shows the local solids concentration and solids velocity profile with different transport velocities. It can be noticed that the solids distribution and flow conditions depend on the transport velocity. At higher transport velocity, the solid particles are all suspended in slurry mixture, and almost uniformly distributed in the pipe cross section, as demonstrated at 4.0 m/s in Fig. 7a, and the solids velocities are almost equal in the pipe cross section. With the transport velocity decreasing, the solid particles in upper part tend to the lower part, and the velocity of solids particles in lower part slowdown, which tends to form a moving bed. Especially at 1.5 m/s, the solid particles clearly accumulate and move in lower part, as demonstrated in Fig. 7b, and the solids velocity in moving bed is lower than upper part.

Figure 8a shows that the local mean solids concentration obtained from ERT and from EMF and CMF are almost same (the measurement error is less than 1%), which implies that the ERT provides a reasonable method to visualize slurry flow. Figure 8b shows that the mean solids velocity obtained from ERT basically keep consistent with the transport velocity at high velocity (especially over 3.0 m/s). However, as the increase of solids concentration in pipe bottom leads to a strong

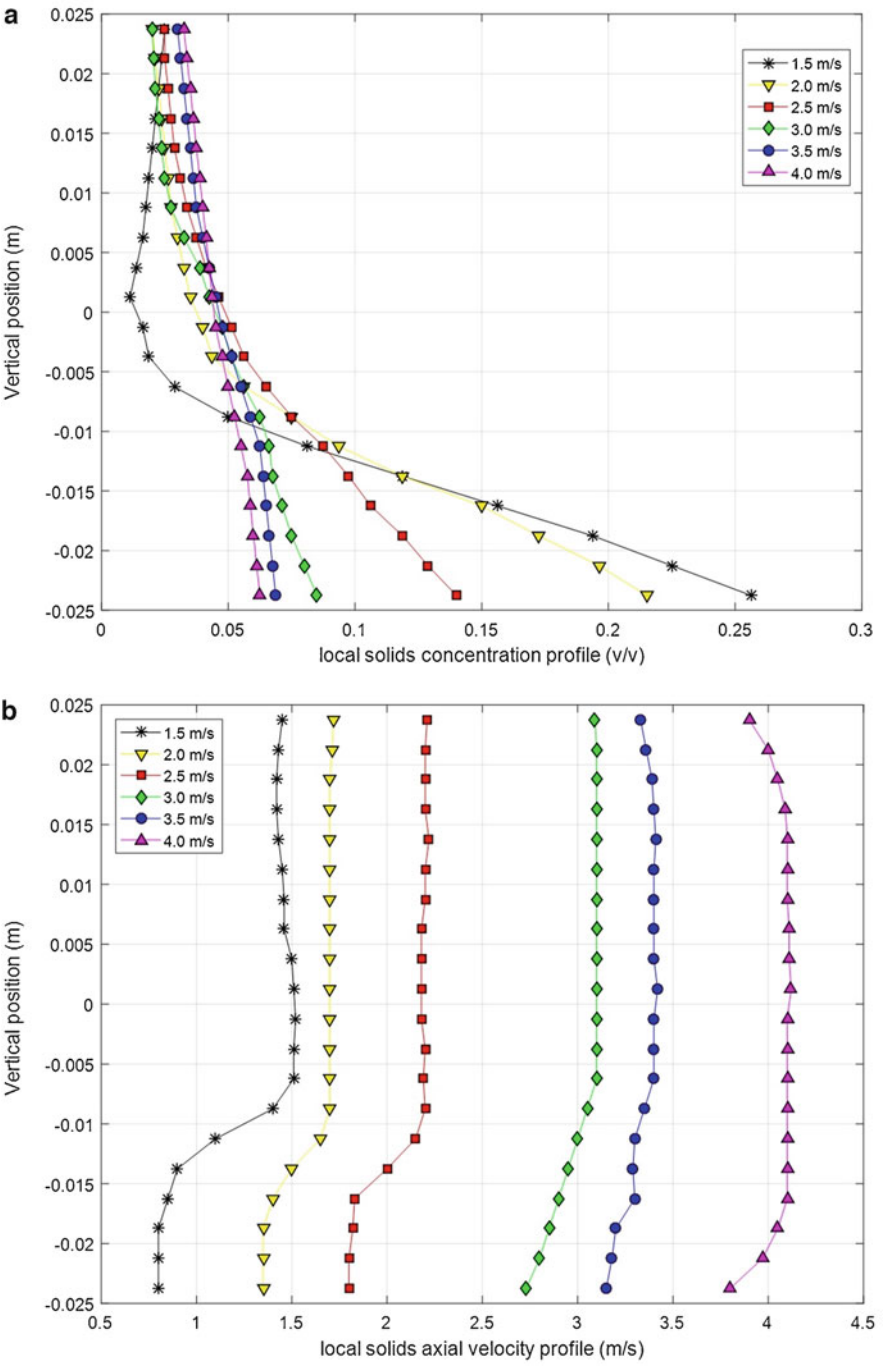

Fig. 6 Visualization of slurry flow with 5% sand (*transport velocities (from 1.5 to 4.0 m/s)*) (**a**) Local solids concentration profile. (**b**) Local solids velocity profile

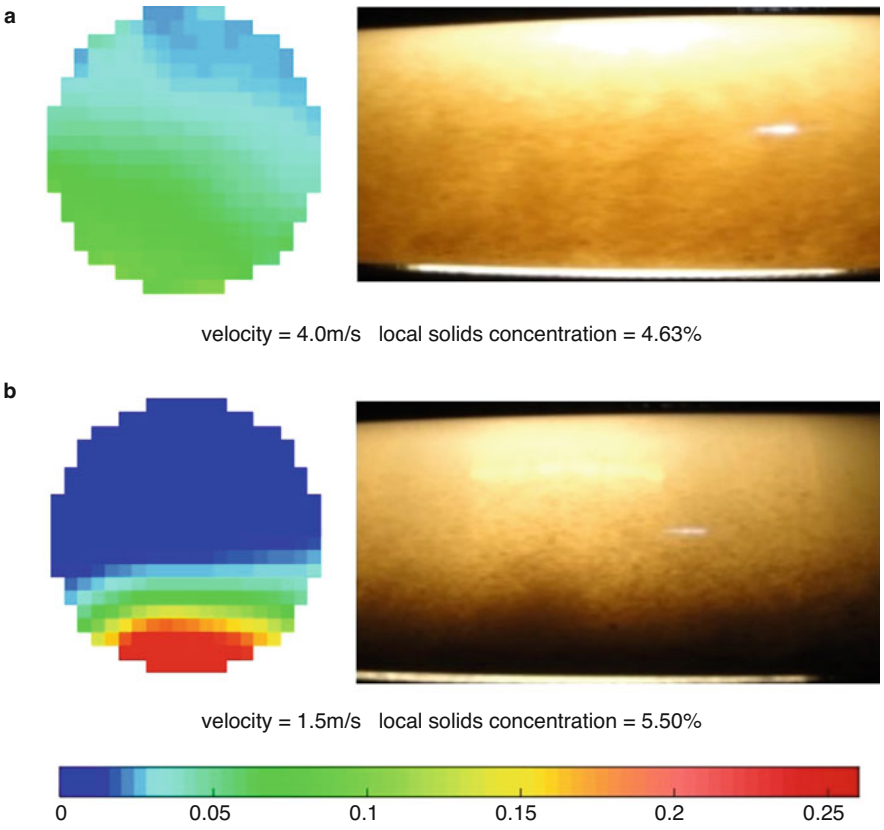

Fig. 7 Local solids concentration distribution of pipe cross section and photography of slurry flow. (**a**) Slurry flow at 4.0 m/s transport velocity. (**b**) Slurry flow at 1.5 m/s transport velocity

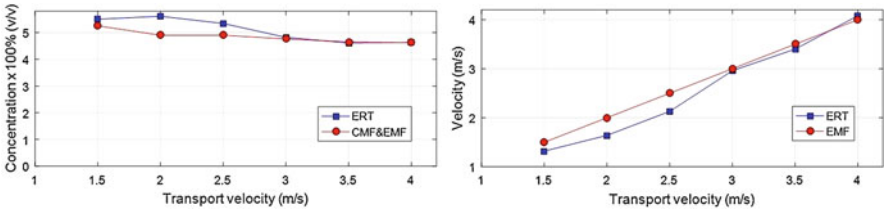

Fig. 8 Error analysis. (**a**) Comparison of local solids concentration obtained from ERT with that of CMF and EMF, (**b**) Comparison of solids velocity obtained from ERT and transport velocity measured by EMF

particle–particle interaction at low velocity (below than 2.5 m/s), the movement of solid particles is impeded, and the solids velocity is lower than transport velocity, which is highlighted by ERT.

6 Conclusions

A visualization method with using a high-performance ERT system on horizontal slurry flow was investigated. It demonstrated ERT can determine the mean local solids concentration and solids concentration profile at vertical positions of pipe cross section, which shows the amount and the distribution of solid particles in slurry. And with cross-correlation technique, the dual-plane ERT system can determine the mean local solids velocity and solids velocity profile in pipe. The ERT results were compared with actual photography and other flow measurement methods, which verified the dual-plane ERT system can perform well for visualizing slurry flow in pipeline. Meanwhile, the below conclusions were drawn:

- Compared with photography and other flow measurement methods, ERT offers a better solution for monitoring slurry flow, as the solids concentration distribution and velocity distribution were clearly shown in ERT results.
- At slow slurry transparent velocity, the solids velocity in lower part of pipe is slower than that in upper part and the mean local solids velocity is smaller than transparent velocity, which are highlighted in ERT results.

Acknowledgments The authors would like to express their gratitude for the support from the Chinese Scholarship Council (CSC) and the School of Chemical and Process Engineering, who made Mr. Li's study at the University of Leeds possible.

References

1. Stanley, S. J., & Bolton, G. T. (2010). A review of recent electrical resistance tomography (ERT) applications for wet particulate processing. *Particle & Particle Systems Characterization, 25*(3), 207–215.
2. Abulnaga, B. (2002). *Slurry systems handbook*. New York: McGraw-Hill. ISBN 0-07-137508-2.
3. Robert, C., & Ramsdell. (2013). An overview of flow regimes describing slurry transport. In *Proceedings of the Art of Dredging, Brussels, Belgium*.
4. Kaminoyama, M. (2014). Review of visualization of flow and dispersion states of slurry system fluids in stirred vessels. *Journal of Chemical Engineering of Japan, 47*(2), 109–114.
5. Shook, C. A., & Masliyah, J. H. (2010). Flow of a slurry through a venturi meter. *Canadian Journal of Chemical Engineering, 52*(2), 228–233.
6. Nasr-El-Din, H., Shook, C. A., & Colwell, J. (1987). A conductivity probe for measuring local concentrations in slurry systems. *International Journal of Multiphase Flow, 13*(3), 365–378.
7. Schmidt, M., Münstedt, H., Svec, M., Roosen, A., Betz, T., & Koppe, F. (2010). Local flow behavior of ceramic slurries in tape casting, as investigated by laser-Doppler velocimetry. *Journal of the American Ceramic Society, 85*(2), 314–320.
8. Shimada, T., Habu, H., Seike, Y., Ooya, S., Miyachi, H., & Ishikawa, M. (2007). X-ray visualization measurement of slurry flow in solid propellant casting. *Flow Measurement & Instrumentation, 18*(5), 235–240.
9. Krupička, J., & Matoušek, V. (2014). Gamma-ray-based measurement of concentration distribution in pipe flow of settling slurry: Vertical profiles and tomographic maps. *Journal of Hydrology & Hydromechanics, 62*(2), 126–132.

10. Stener, J. F., Carlson, J. E., Sand, A., & Pålsson, B. I. (2016). Monitoring mineral slurry flow using pulse-echo ultrasound. *Flow Measurement & Instrumentation, 50*, 135–146.
11. Wang, M. (2015). *Industrial tomography: Systems and applications*. Woodhead Publishing, Limited. ISBN 978-1-78242-118-4.
12. Li, Y., Cao, S., Man, Z., & Chi, H. (2011). Image reconstruction algorithm for electrical capacitance tomography. *Information Technology Journal, 10*(8), 269–291.
13. Wang, M., Wang, Q., & Bishal, K. (2016). Arts of electrical impedance tomographic sensing. *Philosophical Transactions, 374*(2070), 20150329.
14. Wang, M., Jones, T. F., & Williams, R. A. (2003). Visualization of asymmetric solids distribution in horizontal swirling flows using electrical resistance tomography. *Chemical Engineering Research & Design, 81*(8), 854–861.
15. MOSAIC Scientific Ltd. (2009). *AIMFlow Standard Version 1.0 user manual*. MOSAIC Scientific Ltd.
16. Wang, M., Ma, Y., Holliday, N., Dai, Y., Williams, R. A., & Lucas, G. (2005). A high-performance EIT system. *IEEE Sensors Journal, 5*(2), 289–299.